

SANDIA REPORT

SAND2005-3978

Unlimited Release

Printed August 2005

A Joint Computational and Experimental Study to Evaluate Inconel-Sheathed Thermocouple Performance in Flames

Aaron L. Brundage, Sean P. Kearney, A. Burl Donaldson, Vern F. Nicolette, and Walt Gill

Prepared by
Sandia National Laboratories
Albuquerque, New Mexico 87185 and Livermore, California 94550

Sandia is a multiprogram laboratory operated by Sandia Corporation, a Lockheed Martin Company, for the United States Department of Energy's National Nuclear Security Administration under Contract DE-AC04-94AL85000.

Approved for public release; further dissemination unlimited.



Issued by Sandia National Laboratories, operated for the United States Department of Energy by Sandia Corporation.

NOTICE: This report was prepared as an account of work sponsored by an agency of the United States Government. Neither the United States Government, nor any agency thereof, nor any of their employees, nor any of their contractors, subcontractors, or their employees, make any warranty, express or implied, or assume any legal liability or responsibility for the accuracy, completeness, or usefulness of any information, apparatus, product, or process disclosed, or represent that its use would not infringe privately owned rights. Reference herein to any specific commercial product, process, or service by trade name, trademark, manufacturer, or otherwise, does not necessarily constitute or imply its endorsement, recommendation, or favoring by the United States Government, any agency thereof, or any of their contractors or subcontractors. The views and opinions expressed herein do not necessarily state or reflect those of the United States Government, any agency thereof, or any of their contractors.

Printed in the United States of America. This report has been reproduced directly from the best available copy.

Available to DOE and DOE contractors from
U.S. Department of Energy
Office of Scientific and Technical Information
P.O. Box 62
Oak Ridge, TN 37831

Telephone: (865)576-8401
Facsimile: (865)576-5728
E-Mail: reports@adonis.osti.gov
Online ordering: <http://www.osti.gov/bridge>

Available to the public from
U.S. Department of Commerce
National Technical Information Service
5285 Port Royal Rd
Springfield, VA 22161

Telephone: (800)553-6847
Facsimile: (703)605-6900
E-Mail: orders@ntis.fedworld.gov
Online order: <http://www.ntis.gov/help/ordermethods.asp?loc=7-4-0#online>



A Joint Computational and Experimental Study to Evaluate Inconel-Sheathed Thermocouple Performance in Flames

Aaron L. Brundage
Thermal and Reactive Processes

Sean P. Kearney
Thermal/Fluid Experimental Sciences

A. Burl Donaldson, Vern F. Nicolette, and Walt Gill
Fire Science and Technology

Sandia National Laboratories
P.O. Box 5800
Albuquerque, New Mexico 87185-0836

Abstract

A joint experimental and computational study was performed to evaluate the capability of the Sandia Fire Code VULCAN to predict thermocouple response temperature. Thermocouple temperatures recorded by an Inconel-sheathed thermocouple inserted into a near-adiabatic flat flame were predicted by companion VULCAN simulations. The predicted thermocouple temperatures were within 6% of the measured values, with the error primarily attributable to uncertainty in Inconel 600 emissivity and axial conduction losses along the length of the thermocouple assembly. Hence, it is recommended that future thermocouple models (for Inconel-sheathed designs) include a correction for axial conduction. Given the remarkable agreement between experiment and simulation, it is recommended that the analysis be repeated for thermocouples in flames with pollutants such as soot.

Acknowledgments

The authors gratefully acknowledge access to the Laser Diagnostics Laboratory (LDL) and the assistance of Tom Grasser who provided invaluable technical support. Peer review was performed by Cecily Romero and Dean Dobranich. All support is gratefully acknowledged.

Contents

| | |
|--|----|
| Acknowledgements..... | 4 |
| Nomenclature..... | 7 |
| 1. Overview..... | 9 |
| 2. Experimental Setup..... | 10 |
| 3. Experimental Results..... | 12 |
| 3.1 Internal Probe Construction Effects..... | 13 |
| 3.2 Equivalence Ratio Effects..... | 15 |
| 3.3 Probe Diameter Effects..... | 16 |
| 3.4 Axial Conduction Effects..... | 17 |
| 3.5 Surface Oxidation Effects..... | 20 |
| 4. Computational Setup..... | 22 |
| 5. Description of VULCAN Thermocouple Model..... | 25 |
| 6. Computational Results..... | 26 |
| 7. Conclusions and Recommendations..... | 28 |
| 8. References..... | 29 |

Figures

| | |
|---|----|
| Figure 1: Schematic of flat-flame Hencken burner experimental setup..... | 10 |
| Figure 2: Photograph of flat-flame Hencken burner experimental setup..... | 11 |
| Figure 3: Cross-section of an ungrounded mineral-insulated, metal-sheathed (MIMS) probe (ASTM E 2181/E 2181M)..... | 12 |
| Figure 4: Emissivity of oxidized Inconel as a function of temperature as determined by integrating the measured spectrum from 1 to 25 μm at 810 K from a sample prepared by baking in air at 1273 K for one hour..... | 13 |
| Figure 5: MIMS-type thermocouple cross-section and probe dimensions, quantified in Table 1..... | 14 |
| Figure 6: Measured gas and thermocouple temperature over equivalence ratio..... | 16 |
| Figure 7: Thermocouple temperature as a function of sheath outer diameter..... | 17 |
| Figure 8: Thermocouple immersion across burner by (a) variable immersion and (b) fixed immersion at 25 mm from burner edge..... | 18 |
| Figure 9: Transverse profiles of thermocouple temperature above burner surface. Thermocouple inserted from the left ($-x$ -direction)..... | 19 |
| Figure 10: Thermocouple with variable immersion depth across a flame showing (a) starting position and (b) ending position..... | 19 |
| Figure 11: Transient temperature profile of 62 mil diameter thermocouple at flame center..... | 20 |
| Figure 12: Thermocouple (62 mil diameter) cooling due to an increase of probe surface emissivity..... | 21 |
| Figure 13: Computational domain of VULCAN [9] simulation..... | 22 |
| Figure 14: Coarse computational grid of VULCAN simulation (56,316 cells)..... | 24 |

| | |
|--|----|
| Figure 15: Grid resolution study of VULCAN simulation | 24 |
| Figure 16: Predicted steady state velocity and temperature distribution of product plume | 26 |
| Figure 17: Measured and predicted thermocouple temperatures as functions of thermocouple diameter | 27 |

Tables

| | |
|--|----|
| Table 1: Variability in thermocouple radiograph measurements, units in mils [6]. Refer to Fig. 5 for associated dimensions..... | 15 |
| Table 2: Initial conditions of VULCAN [9] fire model | 21 |
| Table 3: Properties of VULCAN virtual thermocouple cell [11]..... | 25 |

Nomenclature

| | |
|------|---------------------------------------|
| CARS | Coherent Anti-Stokes Raman Scattering |
| CPU | Central Processing Unit |
| LDL | Laser Diagnostics Laboratory |
| MIMS | Mineral-Insulated, Metal-Sheathed |
| MgO | Magnesium Oxide |
| RHF | Radiant Heat Facility |
| SNL | Sandia National Laboratories |

This page has been intentionally left blank

1. Overview

In full scale fire experimentation, the use of relatively large diameter (1.5 mm) sheathed thermocouple assemblies is the norm. Large-diameter thermocouples lead to a significant difference between the local gas temperature and the thermocouple reading. It is straightforward to model the phenomenon that is responsible for this difference, and as such, “thermocouple” models either have been or are being incorporated in both Sandia Fire Codes VULCAN and FUEGO. As part of the modeling effort, flame temperature measurements and companion simulations have been made to provide data for validating the thermocouple models in SNL fire codes, and to better understand thermocouple measurements in fire environments.

The thermocouple model in the FUEGO fire code is currently under development. A working model exists in a legacy fire code named VULCAN, and experimental measurements reported herein were used to validate the thermocouple model and to provide a methodology for a similar exercise with the FUEGO code. Additionally, detailed thermocouple and gas temperature measurements provided a clearer understanding of the relationship between a thermocouple and its surroundings. This included elucidating the effects of axial conduction, surface oxidation, and probe construction on the thermal response of Inconel-sheathed thermocouples.

Experimental measurements were conducted in a Hencken burner. A Hencken burner is a flat-flame, nearly-adiabatic burner that is fired with metered quantities of methane and air. Reasons for utilizing this apparatus are: (1) this burner has been highly characterized by coherent anti-Stokes Raman Scattering (CARS) measurements; (2) the burner is now equipped with a sophisticated positioning system for precision movement of the thermocouple in the flame; (3) because of on-site data acquisition and fuel/air metering, it is an ideal test-bed for rapid execution of experiments; and (4) the near-adiabatic flat flame’s thermochemical environment is fully understood and characterized by equilibrium calculations and is an excellent source for model calibration studies.

Comparison of simulation results to test data indicated a mean error of 6% between the thermocouple reading and predicted temperature. This error included the combined effects of axial conduction and thermocouple sheath oxidation uncertainty. It is recommended that additional modeling and experiment be conducted for Inconel-sheathed thermocouples in non-adiabatic, soot-producing flames.

2. Experimental Setup

Flat-flame burners that produce a laminar, premixed flame that is uniform, steady, and nearly adiabatic are widely used to calibrate thermocouples and other physical probes [1]. A flat-flame Hencken burner, as depicted in Fig. 1, was used in the reported experiments. The burner surface consists of hypodermic stainless-steel fuel tubes embedded in a stainless-steel honeycomb matrix through which combustion air flows. The fuel and air rapidly mix near the burner surface resulting in a flat flame which is slightly lifted off the burner. The combination of a lifted flat flame and clean-burning methane fuel results in negligible heat loss to the surroundings and a plume of combustion products that is well-approximated by adiabatic equilibrium; the flame burns clean without the production of soot. A photograph of the experimental setup is shown in Fig. 2.

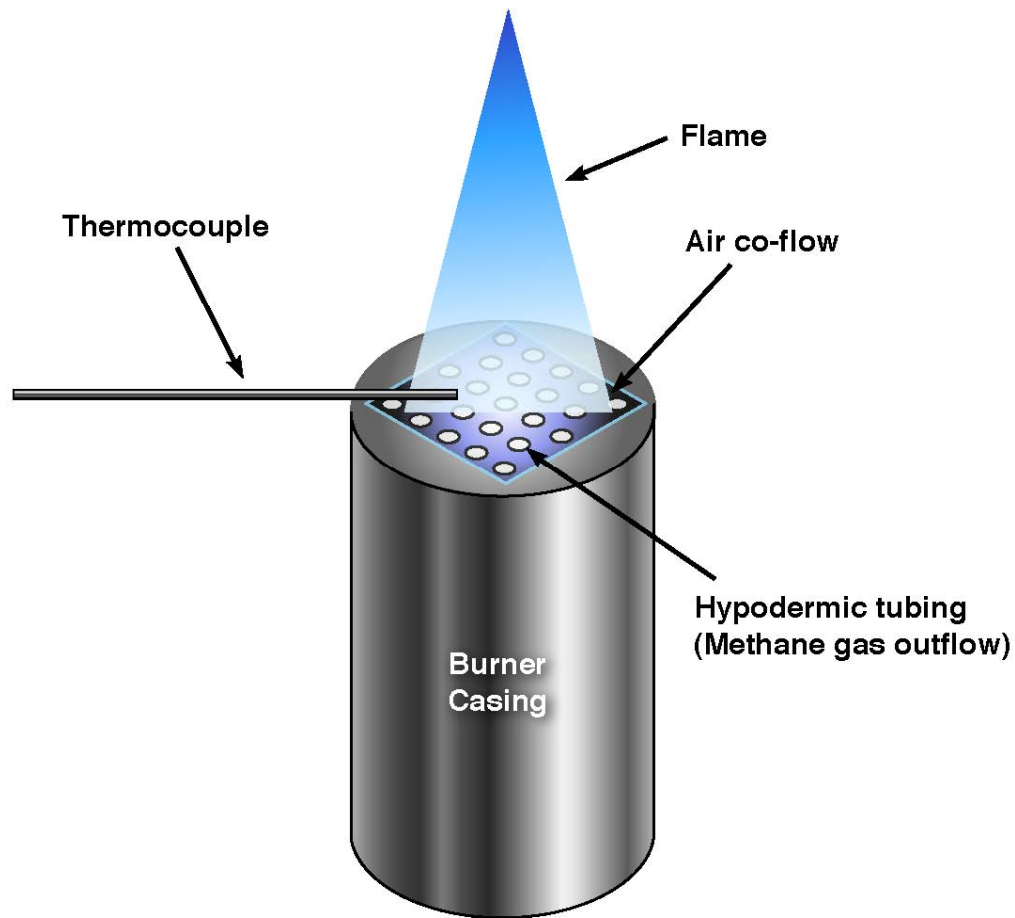


Figure 1: Schematic of flat-flame Hencken burner experimental setup.



Figure 2: Photograph of flat-flame Hencken burner experimental setup.

3. Experimental Results

Flame temperatures are measured across a wide range of equivalence ratios. The equivalence ratio is defined as the ratio of the actual fuel-oxidant ratio to the stoichiometric fuel-oxidant ratio. Coherent Anti-Stokes Raman Scattering (CARS) of the nitrogen molecule was used to measure flame temperature [1]. In addition, readings were observed from 1.0 and 1.6 mm mineral-insulated, metal-sheathed (MIMS) thermocouple probes inserted in the combustion-product plume [2]. A schematic of the MIMS thermocouple probe is shown in Fig. 3. This type of construction is most widely used for high temperature applications and is issued in accordance with the ASTM standard specification for Compacted Mineral-Insulated, Metal-Sheathed, Noble Metal Thermocouples and Thermocouple Cable (E 2181/E 2181M). The thermocouple wires and ungrounded measuring junction are surrounded by a magnesium oxide (MgO) mineral insulation, and the entire assembly is encased in an Inconel 600 sheath. Hence, the transient bead temperature will be dependent upon heat conduction through the probe interior, and the thermal capacitance of the bead, insulation, and sheath.

Inconel is a trade name of the Special Metals Corporation [3]. Inconel 600 is an alloy composed of approximately 72.0% Ni, 14.0 – 17.0% Cr, 6.0 – 10.0% Fe, 0.15% C, 1.0% Mn, 0.015% S, 0.5% Si, and 0.5% Cu. The optical properties of the oxidized Inconel sheath are unknown at the temperatures achieved in the Hencken burner flame. Hence, a range of emissivities was estimated based upon in-house measurements and published data. A lower bound was estimated by oxidizing (at SNL) an Inconel sample at 1273 K, and measuring the spectrum (from 1 to 25 μm) while heating the sample in vacuum at 800 K. By integrating the spectral data with the Planck distribution, a lower bound on the emissivity of 0.67 was calculated at 800 K [4]. Results from this integration are presented in Fig. 4. Based upon other available data for oxidized Inconel 600 [5], the total hemispherical emissivity could be as high as 0.9, and the resulting range of emissivities, from 0.67 to 0.90, will be accounted for in an uncertainty analysis.

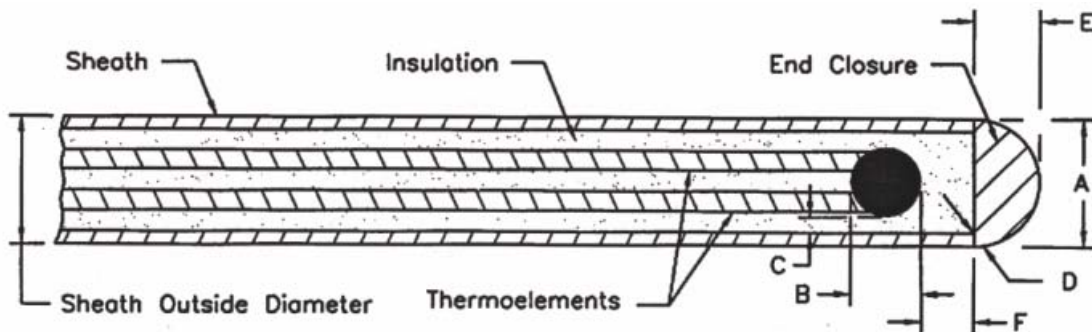


Figure 3: Cross-section of an ungrounded mineral-insulated, metal-sheathed (MIMS) probe (ASTM E 2181/E 2181M).

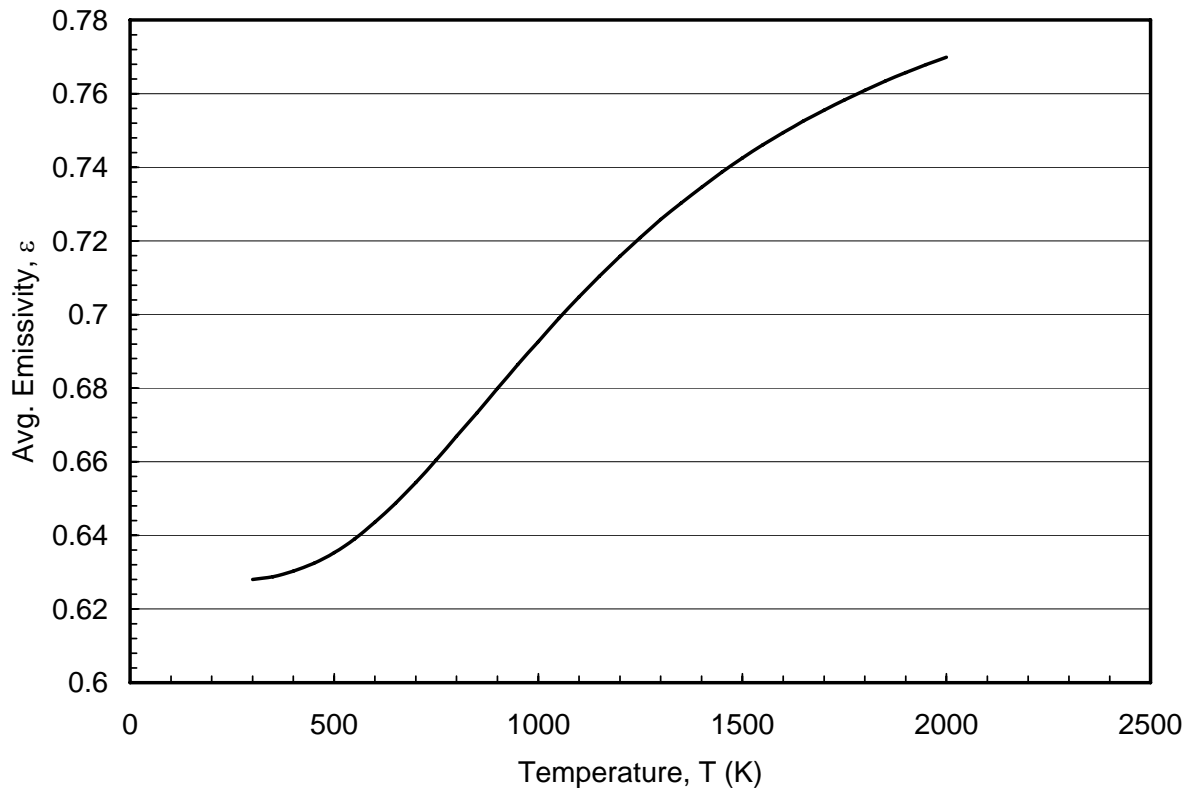


Figure 4: Emissivity of oxidized Inconel as a function of temperature as determined by integrating the measured spectrum from 1 to 25 μm at 800 K from a sample prepared by baking in air at 1273 K for one hour.

To experimentally achieve a stoichiometric flame, i.e. an equivalence ratio of unity, 40 SLPM of air and 3.2 SLPM of methane were passed through the burner to achieve a stoichiometric mass flow rate of 0.0026 kg/s. Using the NASA CEA chemical equilibrium code for an air/fuel mixture initially at 298 K and 0.82 atm, the adiabatic flame temperature was 2220 K and the density of the air-fuel mixture was 0.1239 kg/m³. Given the cross-sectional area of the flat-flame burner (25 cm²) and the density of the air-fuel mixture, the gas velocity was estimated at 8.2 m/s. Various factors contributing to the measured experimental error are quantified in the following subsections.

3.1 Internal Probe Construction Effects

Non-ideal internal probe construction could lead to non-uniform heating and contribute to modeling and experimental uncertainty. Radiographs showing 9 samples from the same manufacturer of Inconel-sheathed, MIMS thermocouples were used to gather the probe internal and external dimensions. A photograph of a machine-sectioned thermocouple tip

is shown in Fig. 5, and the referenced dimensions are tabulated in Table 1. From Fig. 5, it is evident that the insulation terminates before the bead, and that the bead thermally communicates with the sheath across a gap [6]. Based on the tabulated results, the outer diameter of the nominally 62 mil thermocouple is 57 ± 5.6 mil (95% confidence).

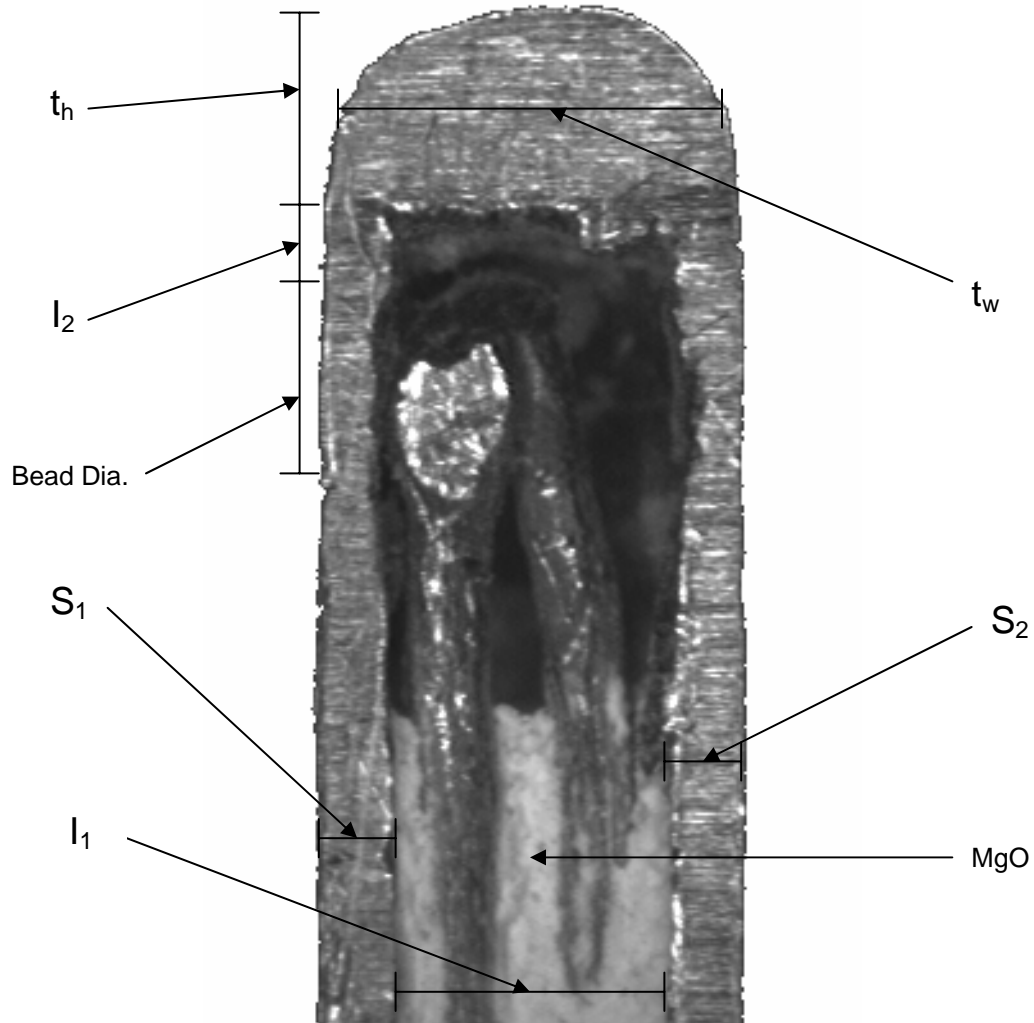


Figure 5: MIMS-type thermocouple cross-section and probe dimensions, quantified in Table 1.

Table 1: Variability in thermocouple radiograph measurements, units in mils [6]. Refer to Fig. 5 for associated dimensions.

| Thermocouple | t_w | t_h | S₁ | S₂ | I₁ | I₂ | Bead Dia. |
|---------------------|----------------------|----------------------|----------------------|----------------------|----------------------|----------------------|------------------|
| 1 | 55 | 30 | 5 | 5 | 45 | 29 | 24 |
| 2 | 57 | 32 | 7 | 8 | 42 | 23 | 25 |
| 3 | 57 | 42 | 7 | 7 | 43 | 24 | 28 |
| 4 | 55 | 37 | 5 | 5 | 45 | 25 | 30 |
| 5 | 54 | 30 | 6 | 5 | 43 | 19 | 25 |
| 6 | 55 | 33 | 6 | 5 | 44 | 30 | 28 |
| 7 | 61 | 36 | 9 | 8 | 44 | 32 | 36 |
| 8 | 57 | 39 | 8 | 7 | 42 | 21 | 26 |
| 9 | 62 | 40 | 8 | 9 | 45 | 25 | 28 |
| Average | 57 | 35 | 6.8 | 6.6 | 44 | 25 | 28 |
| Std. Dev. | 2.8 | 4.4 | 1.4 | 1.6 | 1.2 | 4.3 | 3.6 |

3.2 Equivalence Ratio Effects

CARS-measured flame temperatures were found to be within 50 K of the adiabatic flame temperature, as shown in Fig. 6. Hence, the flame of the Hencken burner is nearly adiabatic, as designed. The thermocouple data tracked the trends of the CARS measurements as the equivalence ratio is varied from lean to rich. Also to be noted is a reasonably consistent suppression of thermocouple indicated temperature below gas temperature. The thermocouple data indicate much lower temperatures (~900 K) than the CARS-measured temperature because of radiant heat loss from the “white-hot” (visible) thermocouple surface to the cold surroundings.

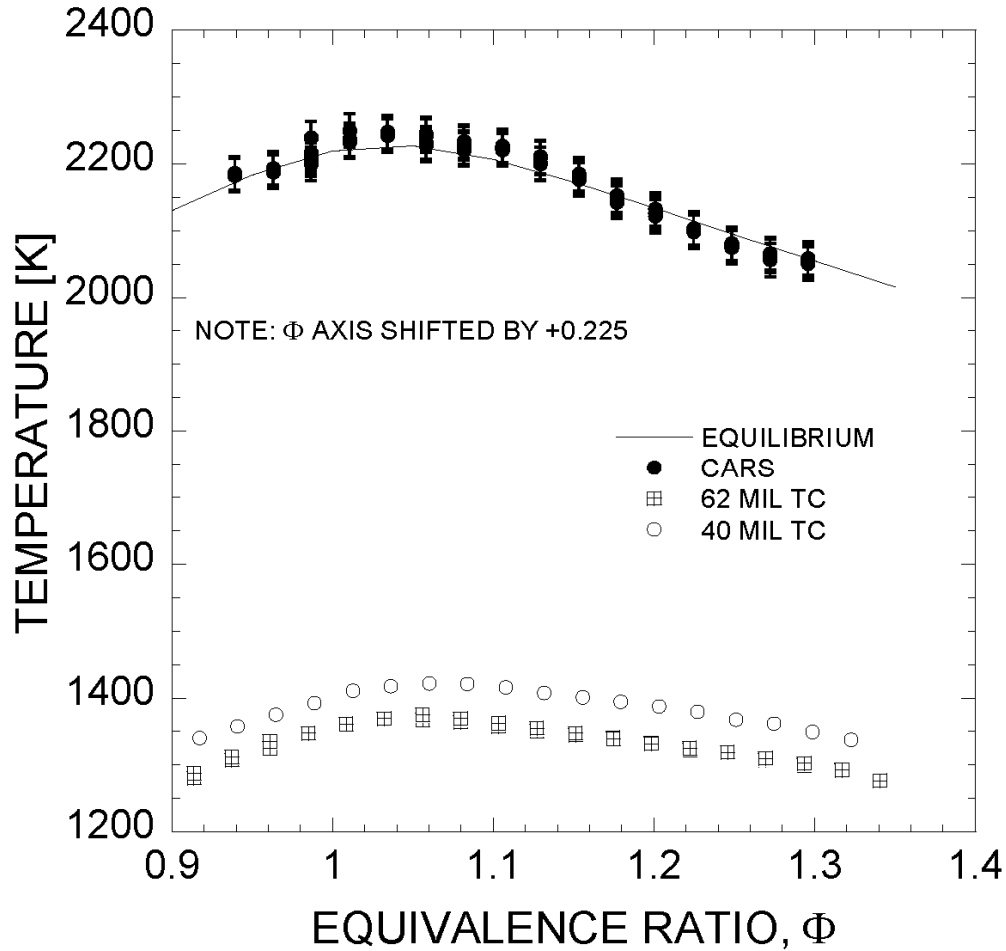


Figure 6: Measured gas and thermocouple temperature over equivalence ratio.

3.3 Probe Diameter Effects

A larger-diameter thermocouple will experience more steady-state radiant heat loss due to a greater surface area. Furthermore, for smaller diameters, the convection heat transfer coefficient becomes exceedingly large and the thermocouple temperature will approach the gas temperature. As shown in Fig. 6, the 1.0 mm diameter thermocouple reached a 50 K-higher steady state temperature than the 1.6 mm diameter thermocouple, with an uncertainty of 0.75% or ± 5 K (95% confidence), based upon the manufacturer's estimate. A more detailed uncertainty analysis of thermocouple measurements is reported by Nakos [7]. As shown in Fig. 7, the influence of thermocouple diameter on recorded temperature was investigated for four thermocouple sizes; the largest three diameters were Inconel sheathed, the smallest diameter was stainless steel sheathed. An interesting feature of this figure is that as diameter approaches zero, the curve can reasonably be extrapolated to the CARS measured gas temperature.

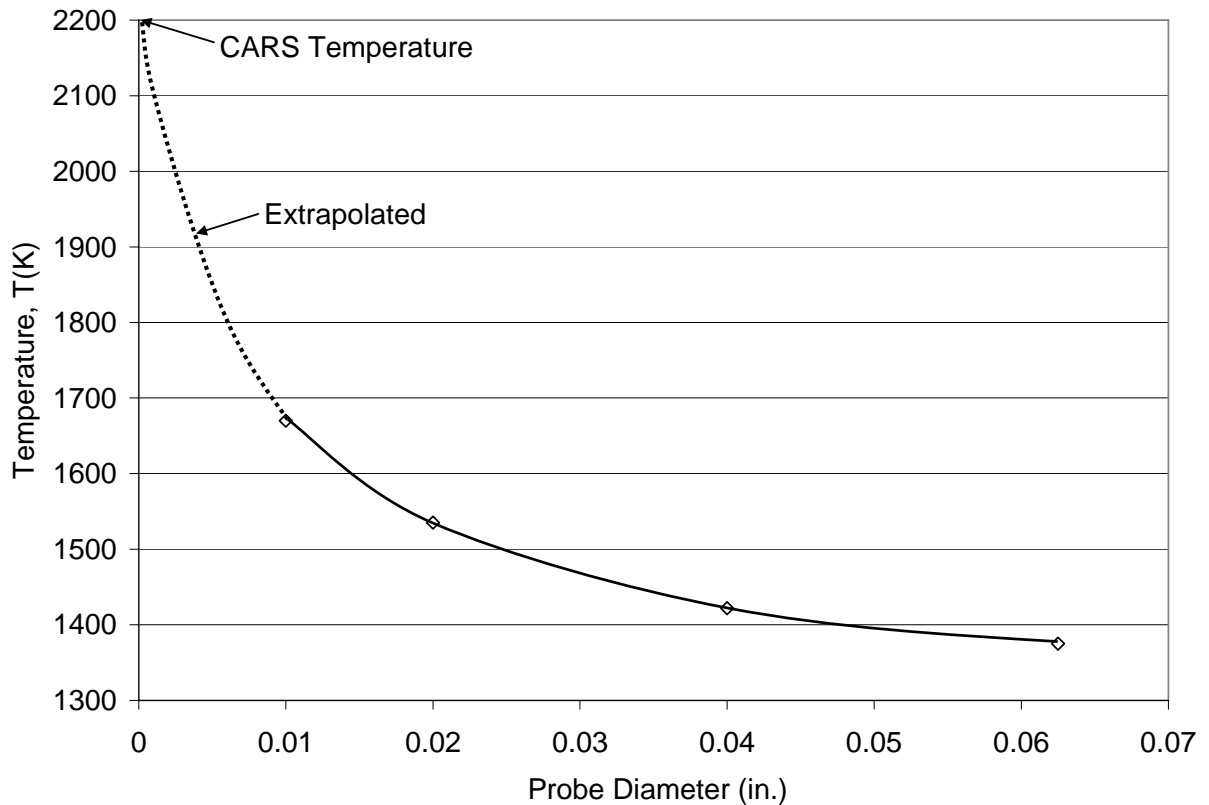


Figure 7: Thermocouple temperature as a function of sheath outer diameter.

3.4 Axial Conduction Effects

A thermocouple inserted near the base of the flame, where the temperature is uniform over a wide area, glows within the flame, as shown in Fig. 2. This suggests that axial conduction along the thermocouple may be important and should be considered as part of the experimental and modeling effort. To illustrate the effects of axial conduction, the thermocouple probe was traversed across the flame by (a) variable immersion and (b) fixed immersion, as shown in Fig. 8. These tests were performed at an equivalence ratio of unity which corresponds to a gas temperature of 2220 K.

Transverse flame temperature profiles from thermocouples of three diameters—10, 62, and 125 mils—are plotted in Fig. 9. The temperature profile from the 10 mil-diameter thermocouple was approximately symmetric about the center of the burner for variable immersion (see Fig. 8(a)). Hence, axial conduction effects are negligible for the small diameter probe. However, for both the 62 mil and 125 mil MIMS thermocouples with variable immersion across the flame, the temperature profiles were asymmetrical. For the probe positions corresponding to variable immersion, as shown in Fig. 10, the thermocouple probe is cooler at Position (a) than at Position (b), when these locations are the same distance from the flame. For Position (b), the thermocouple is heated axially as

it is stretched across the flame; the thermocouple must be extended further across the flame for the temperature to equal that at Position (a).

The temperature profile for a 62-mil diameter thermocouple, inserted across the flame with a fixed immersion depth, as plotted in Fig. 9 and location shown in Fig. 8(b), is symmetric. For this case, the effects of axial conduction are the same at every point along the probe traverse direction. Note that in all cases, there is a response before the thermocouple actually enters the flame (the boundaries of the hot-gas zone do not correspond to the boundaries of the luminous region). Hardee [8] reports that band-emission radiation heating and simple conduction heating are significant heating mechanisms for a thermocouple approaching the edge of the Hencken burner flame.

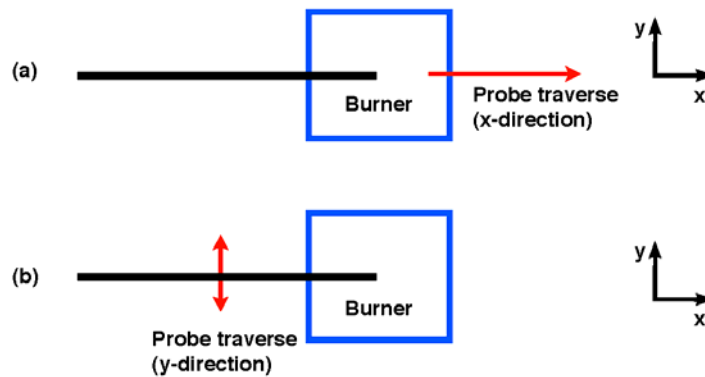


Figure 8: Thermocouple immersion across burner by (a) variable immersion and (b) fixed immersion at 25 mm from burner edge.

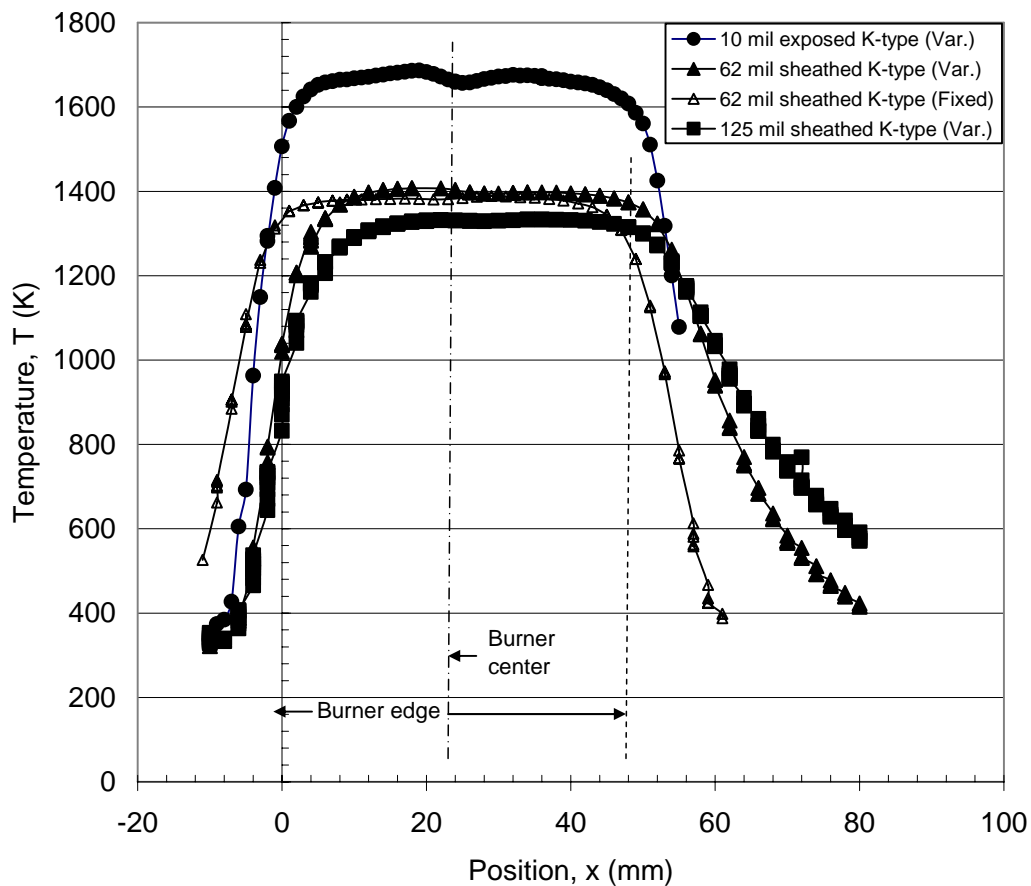


Figure 9: Traverse profiles of thermocouple temperature above burner surface. Thermocouple inserted from the left ($-x$ -direction).

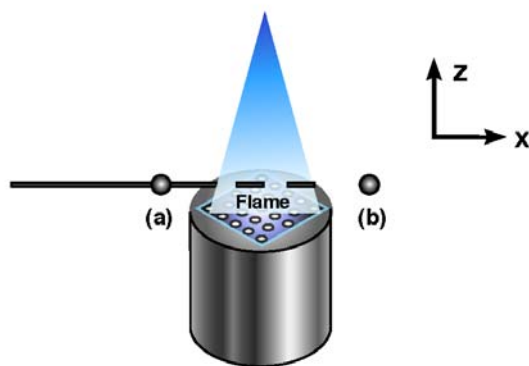


Figure 10: Thermocouple with variable immersion depth across a flame showing (a) starting position and (b) ending position.

3.5 Surface Oxidation Effects

Another experiment was conducted as a simplistic demonstration of both the response time of a thermocouple from initial immersion in the flame, and the cooling due to surface oxidation (and emissivity increase) of the same (initial bright surface) 62 mil thermocouple in the flame. The heat-up from time of insertion into the flame is shown in Fig. 11 and the temperature is seen to stabilize at around 15 seconds. The consequence of the oxidation process can be seen in Fig. 12, beginning with the end point of the data shown in Fig. 11 with re-zeroed time base (note scale changes). The indicated maximum temperature of 1448 K at 15 s (see Fig. 11) dropped to 1404 K at 848 s.

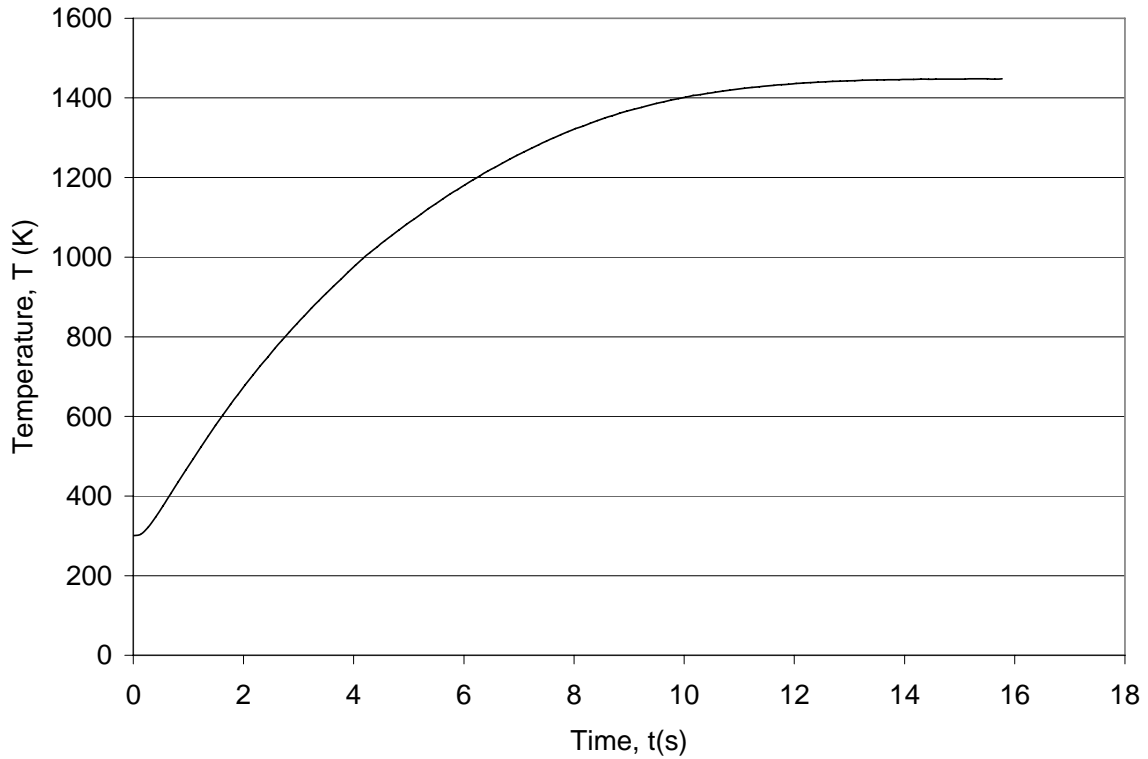


Figure 11: Transient temperature profile of 62 mil diameter thermocouple at flame center.

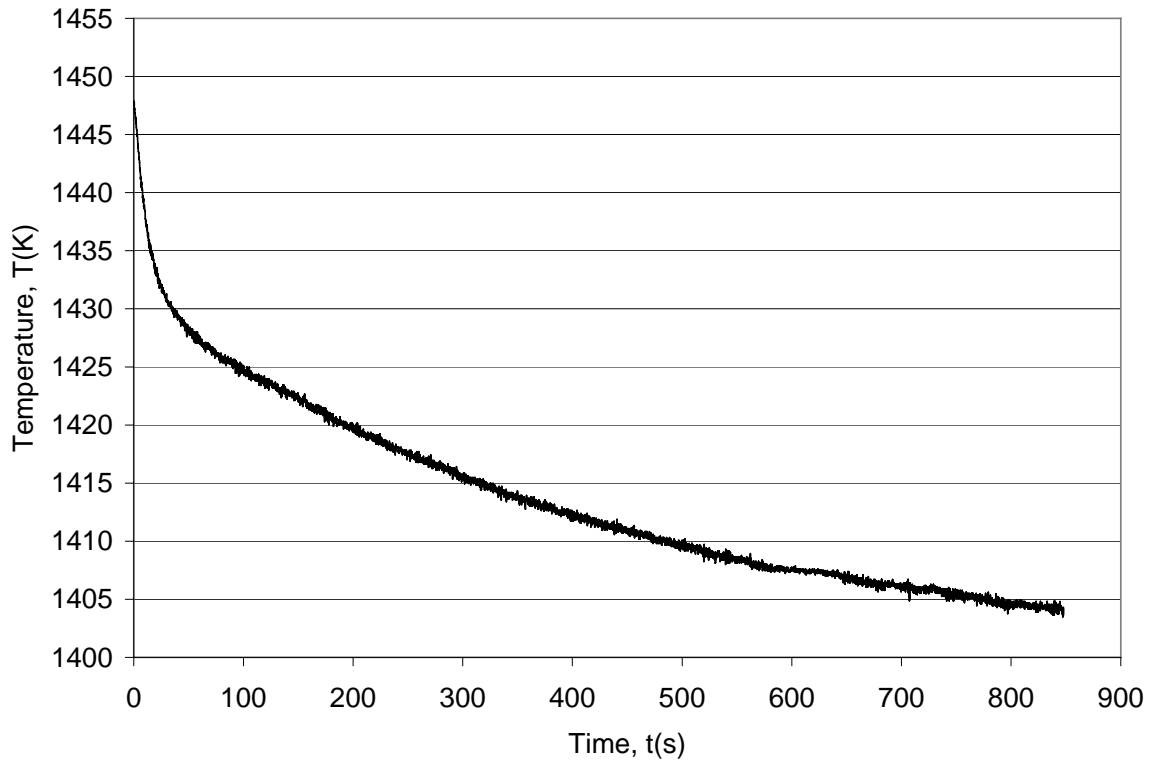


Figure 12: Thermocouple (62 mil diameter) cooling due to an increase of probe surface emissivity.

4. Computational Setup

Given the adiabatic flame temperature, equilibrium species (fuel and air) composition, and approximate gas velocity, a VULCAN [9] simulation of this product plume was constructed, with specific values of these initial conditions provided in Table 2. The computational domain is shown in Fig. 13. Here, the product plume is modeled as a hot gas jet with the equilibrium species composition emanating from the 25 cm² orifice. A virtual thermocouple cell is placed approximately 12 mm above the orifice. Details of the thermocouple model are provided in the next section. Combustion chemistry (ignition in VULCAN) was not modeled. These assumptions are considered adequate for the purpose of evaluating the VULCAN thermocouple model. Any attempts to accurately predict the flame shape from the Hencken burner are beyond the scope of this analysis and the capability of the VULCAN fire code.

Table 2: Initial conditions of VULCAN [9] fire model.

| Parameter | Value |
|-------------------------------------|-------|
| w -velocity, W (m/s) | 8.19 |
| Turbulen kinetic energy, TEK (J/kg) | 0.135 |
| Turbulent dissipation, TED (J/kgs) | 0.815 |
| Temperature, T (K) | 2220 |

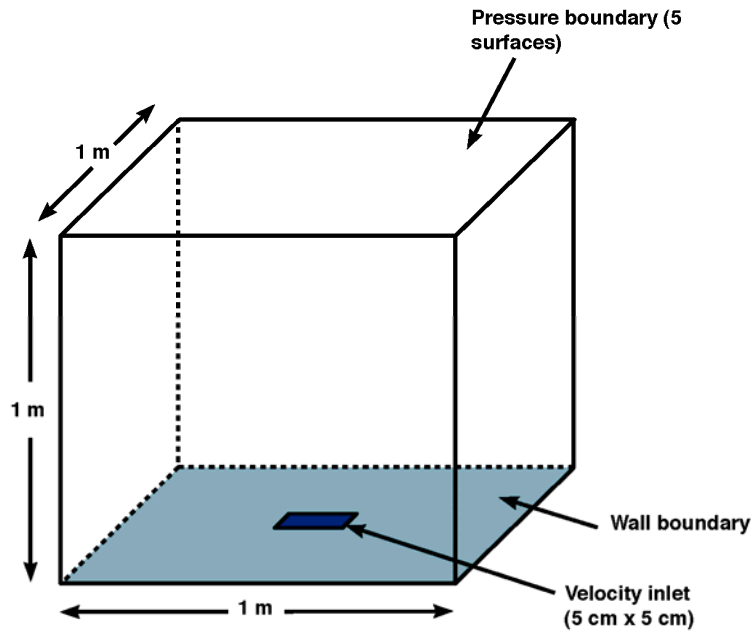


Figure 13: Computational domain of VULCAN [9] simulation.

A structured computational grid with hexahedral bricks was used in the VULCAN model. This computational grid, for the lowest resolution case of 56,316 cells (N_1), is shown in Fig. 14. Other grid resolutions of 181,656 (N_2) and 295,704 cells (N_3) were explored as part of a grid resolution study. Results from a grid resolution study for this version of VULCAN are presented in Fig. 13. For a grid refinement ratio $\sqrt{N_3/N_1}$ of 2.29, the temperature was found to increase by 10K, with most of the increase (9 K) occurring from the second to first refinement level. Although the solution is fully converged at the second refinement level, given the trade-off in CPU time versus accuracy, all results are reported at the lowest resolution (56,316 cells).

Two versions of the VULCAN fire modeling software were applied to this problem. The first version of the code assumed that the inlet boundary could be modeled as a blackbody at the same temperature as the incoming hot gas stream (2220 K). This assumption, which was buried in the code and not obvious, was not appropriate for modeling this particular experiment since the surface of the Hencken burner is relatively cold (at room temperature). Use of the standard version of VULCAN therefore produced an erroneous answer, as it assumed that the thermocouple was affected by thermal radiation from a 2220 K surface equal in area to that of the gas injection stream. The effect was quite large, since the thermocouple was located close to the burner surface. The results obtained with this version of VULCAN are not discussed further, since this version of the model was deemed to not apply to the problem under consideration.

A second version of VULCAN was applied to the problem in which the blackbody assumption on the inlet boundary was turned off. This particular version of VULCAN [10] employed a modified thermal radiation model developed by Alex Brown (9132). Only the injected gases could influence the thermocouple, as well as thermal radiation from the surroundings at room temperature. This version of the code produced a result for the thermocouple temperature that was in good agreement with the data, as shown in the *Computational Results* section.

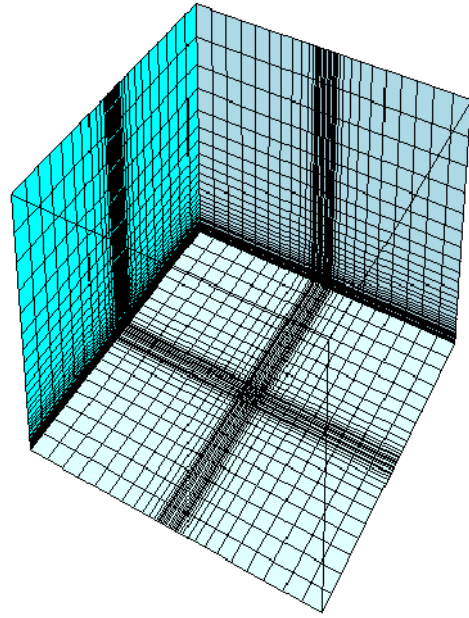


Figure 14: Coarse computational grid of VULCAN simulation (56,316 cells).

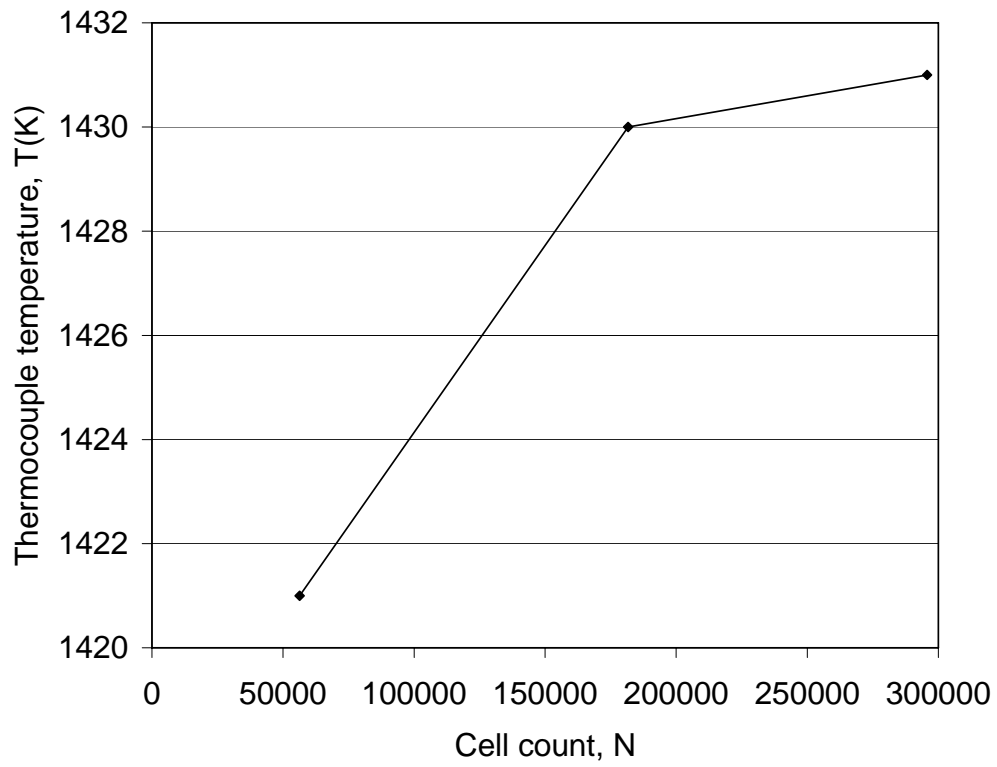


Figure 15: Grid resolution study of VULCAN simulation.

5. Description of VULCAN Thermocouple Model

The VULCAN thermocouple model estimates the temperature that a thermocouple would predict if it were located in the same thermal environment. In the model, only a one-way coupling exists, such that the thermocouple temperature is calculated after the surrounding gas temperature field is predicted. The bead (junction) temperature is calculated assuming radially one-dimensional (1-D), transient conduction. A surface energy balance—equating radiation, convection, and 1-D radial conduction through the hemispherical probe tip—is used to find the surface temperature. A global energy balance and a conduction energy balance are used to determine the centerline transient temperature rise and the centerline temperature, respectively [11]. Hence, the current VULCAN model is for a thermocouple with an exposed junction and lead wires.

Thermal properties of the “virtual” thermocouple, which represent an average of the insulation and sheath properties of a MIMS thermocouple, are provided in Table 3. Although radial conduction at the probe tip is included in the analysis, axial conduction along the axis of the cylindrical portions of the probe (including the Inconel sheath, lead wires and insulation) are ignored. Furthermore, the material properties and thermal capacitances of the bead, insulation, and sheath are lumped. These material property approximations are necessary to apply the current thermocouple model to the MIMS thermocouple used for fire applications here at Sandia National Laboratories (SNL).

A thermal model of a MIMS thermocouple, with geometry representative of an actual thermocouple (see Fig. 5) to determine the bead temperature was reported by Nakos [12]. This model included the air gap around the sheath, assumed lumped masses for the bead and sheath, and considered radiation and conduction as the only (dominant) modes of heat transfer. Results showed that the sheath acted as a radiation shield and reduced the heat transfer to the bead.

Table 3: Properties of VULCAN virtual thermocouple cell [11].

| Parameter | Value |
|------------------------------|--------------|
| Emissivity | 0.67-0.9 |
| Length (cm) | 15 |
| Diameter (mm) | 1.0, 1.6 |
| Density (kg/m ³) | 5880 |
| Thermal Conductivity (W/mK) | 1.7 |
| Specific Heat (J/kgK) | 696 |

6. Computational Results

The predicted steady state velocity and temperature results for the stoichiometric case discussed in Section 4 are shown in Fig. 16. These results are reflective of the modeling intent—to compare the output of the thermocouple model to experiment and to achieve a large region of uniform temperature surrounding the thermocouple. There is remarkable agreement between the thermocouple temperature prediction and observed thermocouple response, as depicted in Fig. 17, with the peak error in the prediction being approximately 6% (or about 90 K), and mean error of approximately 4% (60 K). Since the emissivity of the oxidized Inconel sheath is not quantified in the experiments, the uncertainty is propagated through the numerical results, based upon the published total, hemispherical emissivity of Inconel samples of various alloys. Also, the actual diameters of the thermocouple probes were not measured, and the uncertainty in diameter (from Table 1) is also propagated through the numerical results. Hence, the 95% confidence simulated uncertainty associated with the emissivity and probe diameter does not fully account for the error between measurement and prediction. The overprediction of the bead (junction) temperature is also consistent with the neglect of axial conduction and the lumping of thermal properties in the VULCAN thermocouple model. Although the bead temperatures are overpredicted, the diameter effects (trends) are well reproduced, with the 50 K difference in temperature between the 1.0 and 1.6 mm diameter probes being nearly identical to the measured difference.

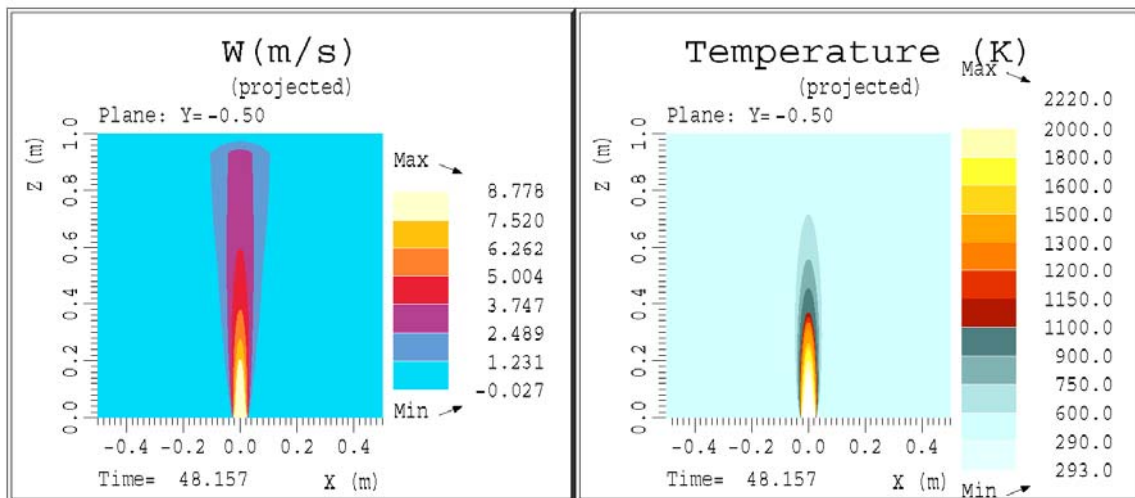


Figure 16: Predicted steady state velocity and temperature distribution of product plume.

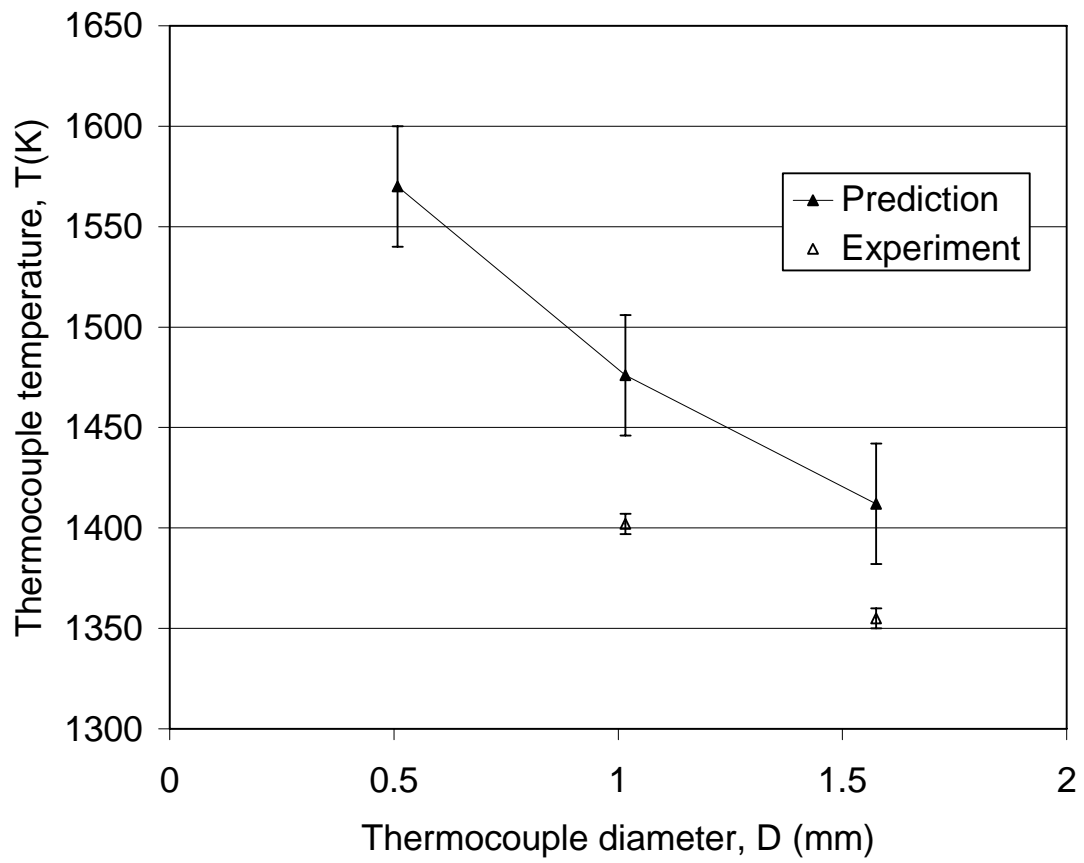


Figure 17: Measured and predicted thermocouple temperatures as functions of thermocouple diameter.

7. Conclusions and Recommendations

It is recommended that future thermocouple models include the effects of axial conduction and thermal property variation to improve current predictive capability for MIMS-type thermocouples. Characterizing the emissivity of the oxidized thermocouple probes and simply measuring the actual probe diameter will reduce the measurement uncertainty. In the present application, the flame was devoid of soot, but most applications at SNL involve flames with soot. Thus, it is additionally recommended that this thermal analysis and companion experiments are repeated for soot-producing flames.

8. References

1. Hancock, R. D., Bertagnolli, K. E., Lucht, R. P., "Nitrogen and Hydrogen CARS Temperature Measurements in a Hydrogen/Air Flame Using a Near-Adiabatic Flat-Flame Burner," *Combustion and Flame*, vol. 109, pp. 323-331, 1997.
2. Donaldson, A. B., "Experimental Data Related to Thermocouple Measurements in a Henken Burner Flame," Sandia National Laboratories Memorandum in Preparation.
3. Special Metals Corporation, "Inconel alloy 600," Publication Number SMC-027, September 2004.
4. Figueroa, V. G., "Emittance of Inconel 600, SS304, 14-4PH Stainless Steel, Aluminum 7075 and Mk4 Aeroshell," Sandia National Laboratories Memorandum to Distribution, Org 09132, Feb 20, 2005.
5. O'Sullivan, J. W., and Wade, W. R., NASA-TN-4121, pp. 1-48, 1957.
6. Black, S., "Geometry and Dimensions of 1/16" Inconel Sheathed Type K Thermocouple," Sandia National Laboratories Memorandum, Org. 9135, July 6, 1998.
7. Nakos, J. T., "Uncertainty Analysis of Thermocouple Measurements Used in Normal and Abnormal Thermal Environment Experiments at Sandia's Radiant Heat Facility and Lurance Canyon Burn Site," SAND2004-1023, April 2004.
8. Hardee, H. C., "Hencken Burner Off-Edge Effect," Sandia National Laboratories Memorandum, July 1, 2005.
9. Holen, J., Brostrom, M., and Magnussen, B.F., "Finite Difference Calculation of Pool Fires, Twenty-Third Symposium (International) on Combustion," The Combustion Institute, pp. 1677-1683, 1990.
10. Brown, A. L., "Memorandum of Record: Corrections to VULCAN to properly predict radiation interactions with symmetry planes," Sandia National Laboratories Memorandum, Org. 9132, August 29, 2002.
11. Gill, W., "Memorandum of Record: Draft Report on Assessment of VULCAN Thermocouple Model," Sandia National Laboratories Memorandum, Org. 9132, March 31, 2005.
12. Nakos, J. T., "The Systematic Error of a Mineral-Insulated, Metal Sheathed (MIMS) Thermocouple Attached to a Heated Flat Surface," Thermal Measurements: The Foundation of Fire Standards, ASTM STP 1427, L. A. Gritzko and N. J. Alvares, Eds., American Society for Testing and Materials, West Conshohocken, PA, 2002.

Distribution:

| | | | |
|---|---------|--------|------------------------|
| 1 | MS-0718 | 06141 | C. Lopez |
| 1 | MS-0825 | 01510 | W. L. Hermina |
| 1 | MS-0836 | 01516 | E. S. Hertel |
| 1 | MS-0836 | 01516 | D. Dobranich |
| 1 | MS-0834 | 01512 | S. M. Trujillo |
| 1 | MS-0834 | 01512 | S. P. Kearney |
| 5 | MS-0836 | 01516 | A. L. Brundage |
| 1 | MS-0836 | 01532 | C. Romero |
| 1 | MS-1135 | 01532 | L. A. Gritz |
| 1 | MS-1135 | 01532 | J. Suo-Anttila |
| 1 | MS-1135 | 01532 | J. Nakos |
| 1 | MS-1135 | 01532 | A. L. Brown |
| 1 | MS-1135 | 01532 | T. K. Blanchat |
| 1 | MS-1135 | 01532 | A. B. Donaldson |
| 1 | MS-1135 | 01532 | V. G. Figueroa |
| 1 | MS-1135 | 01532 | W. Gill |
| 1 | MS-1135 | 01532 | J. C. Hewson |
| 1 | MS-0836 | 01532 | M. N. Jackson |
| 1 | MS-1135 | 01532 | K. A. Jensen |
| 1 | MS-1135 | 01532 | V. F. Nicolette |
| 1 | MS-1135 | 01532 | S. R. Tieszen |
| 1 | MS-0836 | 01532 | W. D. Sundberg |
| 1 | MS-0828 | 01533 | A. R. Black |
| 1 | MS-9018 | 8945-1 | Central Technical File |
| 2 | MS-0899 | 04536 | Technical Library |